Non-Fermi liquid regime in metallic pyrochlore iridates: Quantum Griffiths singularities

Bikash Ghosh,[1] Vinod Kumar Dwivedi,[2,*] and Soumik Mukhopadhyay[1,†]
[1]*Department of Physics, Indian Institute of Technology Kanpur, Kanpur 208016, India*
[2]*Materials Science Programme, Indian Institute of Technology Kanpur, Kanpur 208016, India*

(Received 17 July 2020; accepted 14 October 2020; published 30 October 2020)

We investigate the interplay of Kondo and Ruderman-Kittel-Kasuya-Yosida coupling in the presence of disorder by chemically substituting local moment Cr^{3+} at the Ir sublattice in the metallic $Pr_2Ir_2O_7$. We find evidence of non-Fermi liquid behavior in the transport and thermodynamic measurements at low temperature. Specifically, the magnetic susceptibility exhibits power law divergence at $T = 0$. The nonanalytic temperature and magnetic-field dependence of magnetic susceptibility and the associated scaling suggest the existence of a two-fluid system consisting of a Kondo-screened paramagnetic metal coexisting with magnetically ordered rare regions dominated by interimpurity interaction, similar to the quantum critical Griffiths phase.

DOI: 10.1103/PhysRevB.102.144444

I. INTRODUCTION

Pyrochlore $5d$ iridates $R_2Ir_2O_7$ (R = Y or rare earth elements) [1–9] offer an ideal template to study the interplay of spin-orbit coupling, Coulomb correlation, and the crystal electric field effect in the presence of geometric frustration, potentially leading to the emergence of novel topological electronic and magnetic phases such as Weyl semimetals, chiral spin liquids, etc. An interesting member of this family of compounds is $Pr_2Ir_2O_7$ (PIO), with a non-Kramers doublet ground state for the local moment Pr^{3+}. PIO is supposed to be a two-channel Kondo system with a rich phase diagram [10,11]. However, it was initially proposed that the Kondo coupling is dominated by Ruderman-Kittel-Kasuya-Yosida (RKKY) interaction within the two-impurity Kondo effect framework and that the long-range magnetic order is suppressed not due to Kondo screening but due to the geometric frustration. This turns PIO into a "metallic-spin liquid" [12,13] on a "Kondo lattice" with a partial freezing of spins far below the antiferromagnetic Curie-Weiss temperature [12]. An angle-resolved photoemission spectroscopy study revealed that PIO had three-dimensional quadratic band touching at the Brillouin zone center, which opened up the possibility of realization of non-Fermi liquid (NFL) phases by doping, strain, or confinement effects [14–16]. Recently, it was even suggested that the resistivity minimum of slightly doped biaxially compressed PIO films was a consequence of interplay between decreasing scattering rate and carrier density [16], thus bringing into question the widely held understanding of PIO as a Kondo lattice system.

Similar to other strongly correlated systems, a direct route to investigating the evolution of the quantum phases in pyrochlore iridates is by chemical substitution. Several such studies have already been reported, for example, in Bi-doped $Eu_2Ir_2O_7$ [17], chemical doping of Ca^{2+} for Nd^{3+} in $Nd_2Ir_2O_7$ [18], etc. In PIO, the local moment comes from the Pr^{3+} ion, and conduction electrons are mainly contributed by Ir^{4+} [11,19]. The Kondo (T_K) and RKKY (T_{RKKY}) energy scales are very close to each other in PIO [12]. Chemical substitution in PIO offers us an opportunity to study the NFL behavior, if any, arising primarily due to the competition between the intrasite Kondo and intersite RKKY interactions in the midst of a disordered environment. The ratio of the two energy scales may be tuned by chemically substituting either the Pr^{3+} or Ir^{4+} site. The altered energy scale is expected to provide the driving force for the emergence of novel ground states or, perhaps more importantly, to provide a better understanding of the ground state in the unsubstituted material. The competition between the intrasite Kondo and intersite RKKY interactions within a disordered environment can have profound consequences, especially close to the quantum critical point. In the present paper, we investigate the evolution of magnetic and electronic properties by gradual substitution of Cr^{3+} for Ir^{4+} in PIO. Since Cr^{3+} is a $3d$ magnetic ion, the substitution will bring an extra local moment impurity in the Ir sublattice in addition to already existing Pr^{3+} [19]. Both Kondo and RKKY energy scales are sensitive functions of carrier density [20]: the substitution of Cr^{3+} for Ir^{4+} brings changes in the carrier concentration of the system, which in turn affect the f-d exchange interaction among Ir $5d$ and Pr $4f$ localized spins. Moreover, Cr^{3+}, being lighter than Ir^{+4}, is likely to introduce disorder by modifying the Ir-O bond length and Ir-O-Ir bond angle.

II. EXPERIMENTAL RESULTS AND DISCUSSION

Bulk polycrystalline samples of $Pr_2Ir_{2-x}Cr_xO_7$ (PICO), where $x = 0, 0.05, 0.1, 0.2, 0.3$, were grown by the conventional solid-state reaction route [21–24] using powders of Pr_2O_3, IrO_2, and Cr_2O_3, mixed in their stoichiometric ratios.

*Present address: Department of Physics, Indian Institute of Technology Bombay, Mumbai 400076, India.
†soumikm@iitk.ac.in

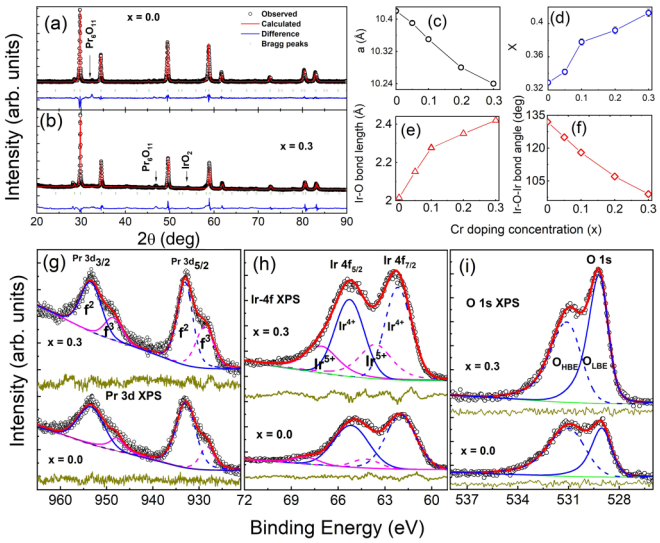

FIG. 1. XRD spectra along with Rietveld refinement recorded at room temperature for $Pr_2Ir_{2-x}Cr_xO_7$ with (a) $x = 0.0$ and (b) $x = 0.3$. Arrows indicate the nominal presence of parasitic phases. (c) Variation of lattice parameter a as a function of x. (d) Variation of positional parameter X as a function of x. Variation of (e) the Ir-O bond distance and (f) the Ir-O-Ir bond angle against x. The XPS spectra of (g) Pr $3d$ for $x = 0.0$ and 0.3, (h) Ir $4f$ spectra for $x = 0.0$ and $x = 0.3$ samples, and (i) De-convoluted O $1s$ peaks for $x = 0.0$ and $x = 0.3$ samples.

The samples were characterized by powder x-ray diffraction (XRD) measurement using a PANalytical XPertPro diffractometer at room temperature. The electrical transport measurement was performed using the conventional four-probe technique. Magnetic susceptibilities were measured by a Quantum Design physical property measurement system. The electronic states were characterized by x-ray photoemission spectroscopy (XPS) using a PHI 5000 Versa Probe II system.

Figures 1(a) and 1(b) show the powder XRD pattern taken at room temperature along with Rietveld refinement using the FULLPROF suite for two representative PICO samples with $x = 0.0$ and $x = 0.3$, respectively. The refinement shows a cubic fcc pyrochlore phase with space group $Fd\bar{3}m$ with no notable changes in terms of the emergence of new peaks or changes in peak position with chemical substitution. The goodness of fit $(=\frac{R_{wp}}{R_{exp}}$, where R_{wp} and R_{exp} are the expected weighed profile factor and the observed weighed profile factor, respectively) value ranges between 2.3 and 8 for all samples. We observe variation in structural parameters with chemical substitution as well. It is expected that a mismatch in the ionic radii between Cr^{3+} (∼0.615 Å) and Ir^{4+} (∼0.625 Å) would lead to changes in structural parameters. The lattice parameters obtained from Rietveld refinement using the FULLPROF suite are plotted in Figs. 1(c)–1(f). The lattice constant a for $x = 0.0$ turns out to be 10.42 Å, which is consistent with the value reported in the literature [25,26]. It decreases with doping of Cr content x, as shown in Fig. 1(c). In the pyrochlore structure, the variable positional parameter X plays a crucial role in controlling the magnetic and electrical transport properties [1,21]. The variation of the positional parameter X as a function of Cr doping content x is shown in Fig. 1(d). The value of X for an ideal IrO_6 octahedron in the pyrochlore structure is 0.3125, where the Ir^{4+} ions are placed under an ideal cubic symmetry [3,21]. The estimated value for the parent sample $x = 0.0$ turns out to be 0.329, which is close to the ideal value. With substitution, the X value is enhanced, indicating more distortion in IrO_6 octahedra. The resultant change in crystal electric field alters the local hybridization between Ir($5d$)/Cr($3d$) and O($2p$) and Pr($4f$) states. The variation of the Ir-O bond length and Ir-O-Ir bond angle as a function of x is shown in Figs. 1(e) and 1(f), respectively. The Ir-O bond length increases with x, while on the other hand, the Ir-O-Ir bond angle is reduced with increasing substitution.

Figures 1(g)–1(i) show XPS spectra taken at room temperature for the two representative samples, $x = 0.0$ and 0.3, of PICO. We fitted the spectrum of Pr $3d$ XPS using a Tougaard-type background [27]. For $x = 0$, fitting suggests a majority of the Pr^{3+} charge state. The Pr $3d$ states are split into two peaks, i.e., Pr $3d_{5/2}$ and Pr $3d_{3/2}$ centered around binding energies of 933 and 953 eV, respectively. The two peaks located at binding energies of 933 eV (main peak) and 928 eV (satellite peak) are labeled f^2 and f^3 states, respectively [28,29]. The ratio of two peaks, i.e., I_{928} (satellite peak)/I_{933}(main peak), turns out to be 0.26 ($x = 0.0$) and 0.5 ($x = 0.3$) for the Pr^{3+} ion, suggesting a sizable fraction of Pr^{+4} charge states along with Pr^{3+} [28]. A rough estimation of the coupling between the conduction electrons and the Pr $4f$ orbital Δ is given by the intensity ratio $r = I(f^3)/[I(f^2) + I(f^3)]$ [27,29,30]. The value of r (0.21 for $x = 0.0$ and 0.35 for $x = 0.3$) increases with Cr substitution, suggesting increased hybridization between the conduction electrons and the Pr $4f$ orbital. The strong mixing of conduction electrons and the Pr $4f$ orbital and the evidence of charge fluctuation as suggested by the existence of Pr^{4+} are characteristic of Kondo systems [27,29,30]. The deconvoluted Ir $4f$ XPS spectra of $x = 0.0$ and $x = 0.3$ samples are shown in Fig. 1(h). We find that the Ir^{4+} charge state is in the majority, while Ir^{5+} is present nominally (∼7%) in the parent sample ($x = 0$). The Ir^{5+} component is increased with substitution (30% for $x = 0.3$). Figure 1(i) shows the O $1s$ spectra with two clearly resolved peaks. The peak situated at lower binding energy (529 eV) is labeled O_{LBE}, and the peak at the higher binding energy (531 eV) is labeled O_{HBE}. The O_{LBE} peak is due to the O^{-2} anion in the system, and the O_{HBE} peak is possibly associated with the presence of O-Pr^{4+} [31].

Figure 2(a) shows the magnetic contribution to the resistivity ρ_m in the absence of magnetic field. There is a rapid increase of ρ_m with increasing x with the ratio $(\Delta\rho)_{max}/\rho_0$ (ρ_0 is the residual resistivity) remaining unchanged, which suggests the dominance of single-impurity scattering in transport. It is also observed that the resistivity minima are shifted towards higher temperature with increasing substitution, implying higher Kondo temperature T_K. In general, the magnetic resistivity follows the generalized Hamann's expression describing potential scattering at each impurity site [32,33]. A clear tendency towards saturation of resistivity at low temperature develops with substitution. The Kondo temperature T_K, extracted from Hamann's fit, increases with increasing substitution, from 7 K for $x = 0$ to 24 K for $x = 0.3$. We calculated residual resistivity ρ_0 by extrapolating Hamann's fit to $T = 0$, which is found to increase with x. A rapidly

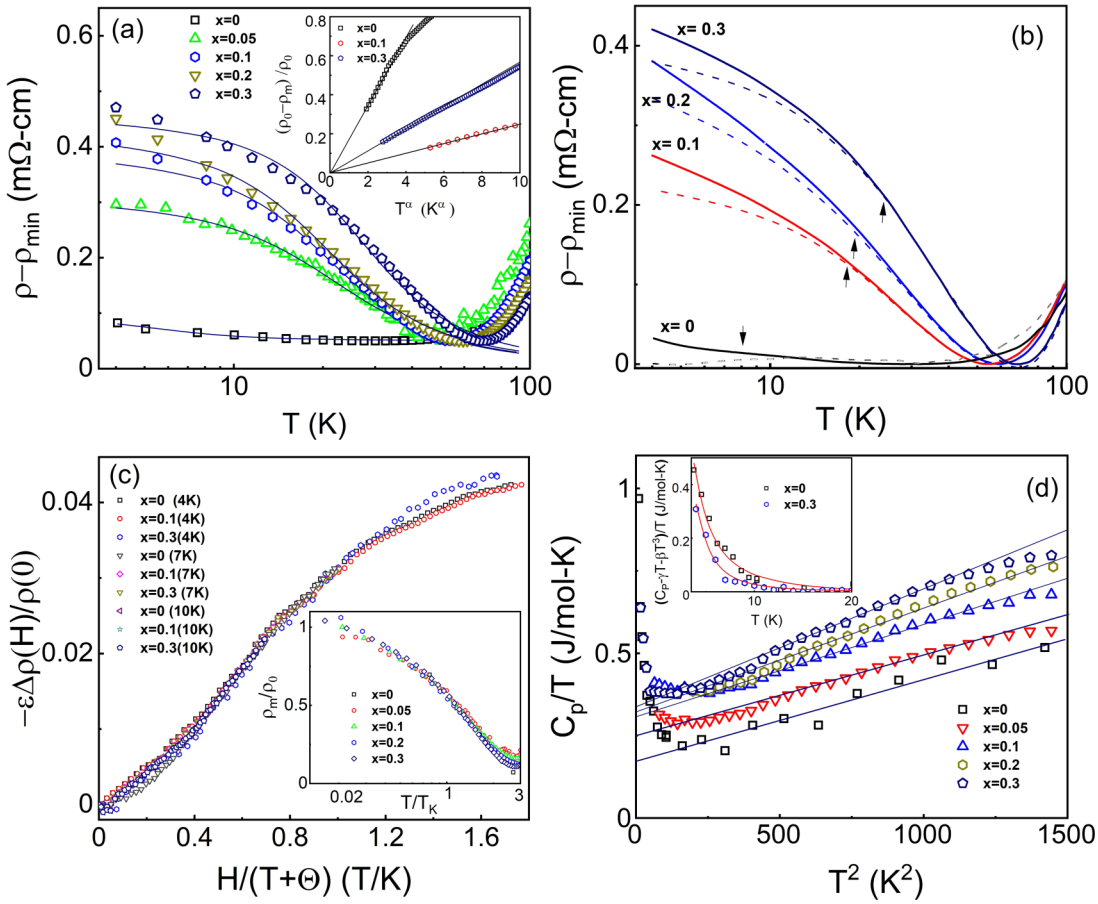

FIG. 2. (a) The temperature dependence of the spin contribution to the resistivity ρ_m of PICO in the absence of magnetic field, where ρ_m is calculated by subtracting resistivity minima $\rho_{\min}$ from $\rho(T)$ at low T, i.e., $\rho_m = \rho(T) - \rho_{\min}$. The Kondo temperature is estimated using Hamann's expression, which is shown by the solid line. Inset: enlarged view of low-T resistivity showing power law divergence. (b) The temperature dependence of resistivity in the absence and in the presence of magnetic field showing suppression of the resistivity upturn with magnetic field. The dashed lines correspond to a magnetic field of 5 T. The locations of T_K are shown by arrowheads. (c) The magnetoresistance (MR) as a function of H/T for the three representative samples showing universal scaling. Inset: The magnetic resistivity ρ_m divided by residual resistivity ρ_0 plotted against normalized temperature T/T_K for various x are found to overlap with each other, demonstrating the existence of a universal scaling. (d) Specific heat divided by temperature C_P/T is plotted against T^2 for various x. The straight lines passing through the data points are linear fits with $\gamma + \beta T^2$. Inset: The NFL component at low temperature plotted for $x = 0$ and $x = 0.3$. The solid lines are guides to the eye.

rising ρ_0 is expected, and it is mainly due to increasing Ir substitution by magnetic Cr. At still lower temperature, we observe a deviation from Hamann's fit below around 6 K. In fact, the resistivity seems to follow the power law at very low temperature, as shown in the inset of Fig. 2(a) with the exponent ranging between 0.7 and 1.2, suggesting non-Fermi liquid behavior. However, the temperature range of the deviation from T^2 behavior is too small to arrive at a definite conclusion. For example, the residual resistivity ρ_{0P} estimated from the power law fit is only slightly higher than that estimated from Hamann's fit ρ_{0H} (Table I).

In Fig. 2(b), we show the temperature dependence of resistivity at low temperature in the presence of magnetic field. For $x = 0$, the resistivity upturn is almost completely suppressed, leading to negative magnetoresistance (MR). For $x \neq 0$, the MR becomes negligible roughly above the Kondo temperature and increases with a decrease in temperature. The appearance of negative MR at temperatures far below T_K could be due to the contribution by the NFL component at low temperature. The maximum value of negative MR observed at the lowest measured temperature is actually reduced marginally with substitution (Table I). It turns out that the MR is a universal function of H/T for all x [Fig. 2(c)], which is again a characteristic of Kondo systems [34,35]. The parameter Θ used in MR scaling has a value in the range 0.1–0.2 K. Another standard experimental signature of the Kondo screening effect is the universal scaling of Kondo resistivity [34–37]. The inset of Fig. 2(c) shows ρ_m/ρ_0 as a function of T/T_K for all x, overlapping with each other below the resistivity minima.

We performed specific heat C_p measurement at low temperature. The specific heat increases as a function of Cr concentration. In the temperature range 15–35 K, C_p/T varies linearly with T^2, as shown in Fig. 2(d). The solid lines are linear fits with $\gamma + \beta T^2$, where γ is the linear coefficient. The linear coefficient γ is determined from the intercept of the linear fit with the vertical axis at $T = 0$. The extracted γ value from the intercepts increases with an increase of x, as shown in Fig. 2(d) and Table I. The γ value is about 500

TABLE I. Important physical parameters obtained from the magnetization, transport, and specific heat measurements.

x	$-\theta_{CW}$ (K)	μ_{eff}^{exp} (in units of μ_B)	μ_{eff}^{theo} (in units of μ_B)	ξ_L	ξ_H	α	T_{irr} (K)	χ_0 (emu/mol)	T^* (K)	T_K (K)	ρ_{0H} ($m\Omega$ cm)	ρ_{0P} ($m\Omega$ cm)	$-\frac{\Delta\rho_{max}(7T)}{\rho(0)}$ (at 4K)	γ (mJ/mol K)	β (10^4J/mol K^3)
0.0	19	5.38	5.06	0.74(4)		0.7		0.015		7	0.03	0.04	0.04	165	1.67
0.05	27	6.04	5.14	0.70(6)	0.82(1)	0.7		0.004	95	18	0.32	0.36	0.04	236	2.16
0.1	33	5.44	5.21	0.50(4)	0.88(2)	1.2	235	0.001	184	19	0.37	0.41	0.02	300	2.40
0.2	40	6.06	5.35	0.67(5)	0.84(1)	0.9	238	0.002	185	20	0.41	0.47	0.04	310	3.04
0.3	45	6.07	5.50	0.63(5)	0.85(1)	0.7	236	0.011	172	24	0.45	0.51	0.02	332	3.25

times larger for $x = 0.3$ than in copper. The high value of the linear coefficient for all samples confirms quasiparticles gaining heavy thermodynamic mass with Cr substitution. The second term in the linear fit is due to the phonon contribution to the specific heat, with β being a constant related to the Debye temperature (Table I). Interestingly, at low temperature C_P/T increases sharply with lowering of the temperature, again suggesting NFL behavior at low temperature. The non-Fermi liquid component is estimated by the total specific heat minus the linear T and T^3 components, as plotted in the inset of Fig. 2(d). The NFL component is marginally reduced with substitution compared to $x = 0$ [inset in Fig. 2(d)].

The temperature dependence of the field-cooled (FC) and zero-field-cooled (ZFC) magnetic susceptibility is shown in Fig. 3(a). For the parent compound ($x = 0$) as well as for $x = 0.05$, there is no appreciable bifurcation between FC and ZFC susceptibilities down to the lowest measured temperature (3 K), as shown in the inset of Fig. 3(a). As the substitution is increased further, there is clear evidence of opening up of irreversibility in the FC and ZFC curves below a certain temperature T_{irr} (Table I) without any peak in the ZFC curves. The bifurcation is not as pronounced as observed in spin glass systems (that is why a semilog plot is used). We analyzed magnetic susceptibility of the parent compound ($x = 0$) at different temperature regimes using the Curie-Weiss (CW) law: $\chi(T) = \chi_0 + C/(T - \theta_{CW})$, where C and θ_{CW} are the Curie constant and Weiss temperature, respectively. The temperature-independent term χ_0 is attributed to the Van Vleck and Pauli paramagnetic contribution due to Ir $5d$ conduction electrons. For $x = 0$, the high-temperature effective local magnetic moment turns out to be $\mu_{eff} = 3.70\mu_B$/Pr, which is very close to the effective moment of $3.58\mu_B$/Pr expected for isolated Pr^{+3} ions. The negative $\theta_{CW} \sim -19$ K) arises due to effective antiferromagnetic RKKY interaction among the Pr $4f$ moments. Again, μ_{eff} and θ_{CW} are determined by a CW fit in the region 2.5–20 K, which gives diminished values $2.6\mu_B$ and -0.8 K, respectively, indicating Kondo screening of Pr $4f$ moments. The μ_{eff} and θ_{CW} for the samples with $x \neq 0$ are calculated by CW fit in the high-temperature regime. It is found that θ_{CW} is higher for $x \neq 0$ compared to that for $x = 0$. It is also observed that μ_{eff} increases with Cr substitution (Table I). This enhancement in μ_{eff} is expected as Cr^{3+} possesses a large (local) moment ($\mu_{Cr^{3+}} = 3.9\mu_B$).

Given the irreversibility in substituted compounds, it was necessary to measure isothermal magnetic relaxation at low temperature. The samples were zero field cooled, and after the desired temperature was reached, a dc magnetic field of 0.1 T was switched on, and the evolution of magnetization was measured as a function of time. Figure 3(b) shows the time dependence of normalized magnetization for a representative substituted compound $x = 0.3$ compared with

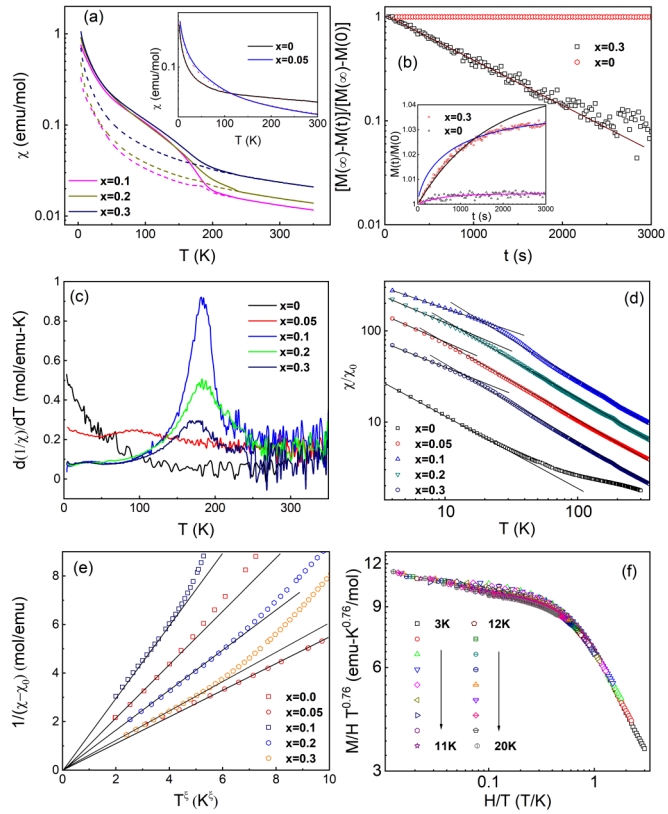

FIG. 3. (a) Semilog plot of dc magnetic susceptibility $\chi(T)$ of $Pr_2Ir_{2-x}Cr_xO_7$ ($x = 0.1, 0.2, 0.3$), showing the irreversibility in FC and ZFC susceptibilities. The dashed lines represent ZFC $\chi(T)$, while FC $\chi(T)$ is represented by solid lines. Inset: $\chi(T)$ for $x = 0, 0.05$ show the absence of bifurcation in ZFC and FC data. (b) Time dependence of normalized magnetization $[M(\infty) - M(t)]/[M(\infty) - M(0)]$ for the two representative samples $x = 0.0$ and $x = 0.3$ at 5 K showing pure exponential relaxation at lower timescales in the semilog plot. Inset: The normalized magnetization is fitted with a pure exponential function at the shorter timescale and a stretched exponential function at the longer timescale. The extrapolated fits in the two regions are shown by solid lines. (c) Temperature derivative of inverse FC susceptibility showing evolution of the maximum with substitution. (d) Log-log plot of χ/χ_0 as a function of temperature showing the power law divergence of the susceptibility. (e) $1/\chi - \chi_0$ tends to zero as T approaches zero. (f) The scaling plot of $(M/H)T^{\xi_L}$ against H/T for $x = 0$.

that for $x = 0.0$. After 3000 s, the percentage change in $M(t)/M(0)$ is 0.4% for $x = 0$, while the same for $x = 0.3$ is 3.2% for $= 0.3$. Long-time magnetic relaxation due to the spin glass or Griffiths phase is generally described by a stretched exponential function $M(t) = M(0) + [M(\infty) - M(0)][1 - \exp\{-(t/\tau)^{\beta}\}]$ [21], where τ is the characteristic relaxation time and β is the stretching exponent which determines the shape of the magnetic relaxation. We observe a pure exponential time relaxation *at the shorter timescale* with the value of β being close to unity for $x = 0$ and 0.3, as demonstrated in the semilog plot [Fig. 3(b)]. Such a time relaxation seems to suggest the formation of magnetically ordered regions with strong spin fluctuation at low temperature. For substituted samples, the slope of the straight line is reduced considerably with increasing temperature and becomes negligible above 15 K (not shown), suggesting the influence of thermal activation as well. The deviation from pure exponential behavior is not clearly discernible from the semilog plot. However, on closer inspection, a deviation from the pure exponential behavior at the longer timescale is indeed observed from the fit of normalized relaxation data in the linear scale [inset in Fig. 3(b)]. We have introduced piecewise fitting of the data using the pure exponential function at the lower timescale and stretched exponential function at the larger timescale, with subsequent extrapolations [shown by the solid lines in the inset of Fig. 3(b)]. Above 1300s, the $M - t$ data can be best fit with a stretching exponent β value of 0.65 for $x = 0.3$. Using the same method, we found nonexponential relaxation with the value of the stretching exponent $\beta = 0.70$ at 10 K (not shown). Such nonexponential relaxation at the long timescale could be attributed to the spin glass or Griffiths phase. The temperature derivative of inverse field-cooled susceptibility is plotted in Fig. 3(c). A well-defined extremum develops for $x \geqslant 0.1$, suggesting magnetic order. In fact, the evolution of the extremum is not abrupt as a faint broad extremum is also observed for $x = 0.05$ [Fig. 3(c)]. These extremum points are labeled T^* and are listed in Table I.

Figure 3(d) shows a log-log plot of ZFC χ/χ_0 vs T for all samples. As discussed earlier, the value of χ_0 has been determined by a CW fit in the paramagnetic regime at high temperature. The susceptibility follows power law divergence $\chi \sim T^{-\xi}$. From Fig. 3(d), it is clear that at low temperature, the power law exponent is sensitive to x, while on the other hand, at high temperature, the variation of ξ with x is practically minimal. Interestingly, for $x = 0$, the power law behavior is limited to low temperature. For nonzero x, we observe two power law exponents: one at low temperature (ξ_L) and the other at high temperature (ξ_H). The exponents are summarized in Table I. One of the possible reasons for the difference in low-temperature and high-temperature power law exponents for $x \neq 0$ (with ξ_L always being smaller than ξ_H) might be increased Kondo screening of the local moments.

Power law divergence can arise due to enhanced spin fluctuation [38], critical valence fluctuations [39], or heavy quasiparticles coupling with the spin fluctuation in the vicinity of a local quantum critical point and getting destroyed in the process [40]. However, in this case, the magnetic instability, as identified by the irreversibility in the ZFC and FC susceptibilities, the extremum in the temperature derivative of the FC susceptibility, and power law divergence of the ZFC

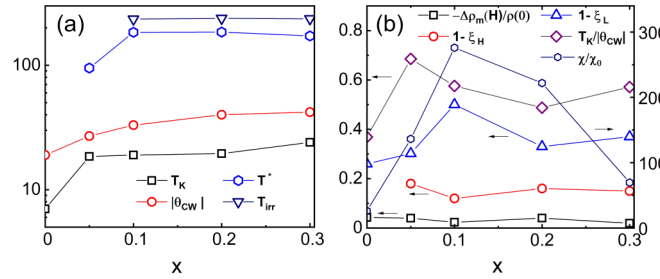

FIG. 4. (a) Variation of important temperature scales T_K, $|\theta_{\rm CW}|$, T^*, and T_{irr} with x. (b) The dimensionless quantities such as the power law exponents ξ_L and ξ_H, $\frac{\chi}{\chi_0}$ (at 4 K), $\frac{T_K}{|\theta_{\rm CW}|}$, and the maximum value of negative MR plotted against x.

susceptibility, sets in at a much higher temperature scale compared to the respective Kondo temperatures for all samples (Table I). The magnetic instability thus does not emerge from the heavy Fermi liquid. It is not associated with a breakdown of Kondo effect either as the ratio χ/χ_0 is eventually reduced with increasing substitution [Fig. 4(b) and Table I].

We also test the divergence of χ at $T = 0$ by plotting the inverse of $\chi - \chi_0$ against T^{ξ} at low temperature and extrapolating the same to $T = 0$ [Fig. 3(e)]. We find no finite intercept on the $T = 0$ axis for all x, thus confirming that the susceptibility truly diverges at $T = 0$, going by the trend down to 3 K. The magnetization at nonzero temperature T and magnetic field H exhibit a scaling behavior of $(M/H)T^{\xi_L}$ as a universal function of H/T^{β}, characteristic of NFL systems [41–43]. The H/T^{β} scaling is observed over several decades, as shown for $x = 0$ in Fig. 3(f). For $x = 0$, the best collapse of data points is observed in the range $\beta = 1 \pm 0.1$ and $\xi_L = 0.76 \pm 0.03$. A change in $\beta > 0.1$ and $\xi_L > 0.04$ in either direction results in a larger spread of data points than what is plotted in the Fig. 3(f). Power law divergence of magnetic susceptibility χ, specific heat C, and resistivity ρ is observed in the case of single-impurity fluctuations in a multichannel Kondo system where the power law exponent is associated with the conduction electron channel number [44]. The power law scaling can also be attributed to Griffiths singularities arising out of the interplay between RKKY and Kondo interactions in a disordered Kondo lattice, close to the quantum critical point [45]. The competition between RKKY interaction, which favors long-range order, and the Kondo effect, which leads to quenching of magnetism or the local Fermi liquid, in the presence of disorder, could lead to magnetically ordered rare regions in the metallic paramagnetic matrix, similar to the Griffiths phase in dilute magnetic systems. The scaling dimension β is a reliable indicator of the origin of NFL behavior. If the value of β is greater than unity, the scaling suggests interimpurity interaction near the quantum critical point, whereas a β value of less than unity suggests the single-impurity multichannel effect [46]. In this case, it is difficult to rule, based on the scaling alone, in favor of either the single-impurity multichannel effect or interimpurity interaction, as β is centered around 1 with an uncertainty of ± 0.1. However, fortunately, at least the sample with $x = 0$ is capable of exhibiting only a single-impurity two-channel Kondo effect due to mixing between the Pr^{3+} non-Kramers doublet ground state and the Kramers doublet

excited state. A two-channel Kondo effect is supposed to show logarithmic divergence in susceptibility and not power law divergence. So we can safely conclude that even for $x = 0$, interimpurity interaction plays a dominant role, leading to power law divergence of susceptibility *at low temperature*. For $x \neq 0$, the substitution of the Ir site by Cr^{3+} increases the local moment concentration, which leads to enhanced influence of the interimpurity interaction. This is reflected in the power law behavior in magnetic susceptibility extending to higher temperature compared to $x = 0$.

We plot the variation of relevant temperature scales and certain dimensionless quantities with substitution x in Figs. 4(a) and 4(b), respectively. We recall from Fig. 1(c) that the unit cell volume decreases with increasing x. Surprisingly, we observe that both T_K and $|\theta_{CW}|$, which sets the energy scale for the RKKY interaction, are enhanced with substitution. The relatively higher percentage increase of T_K compared to the increase of T_{RKKY} with chemical substitution [Fig. 4(b)] should, on the face of it, inhibit magnetic order due to enhanced quantum fluctuation. The resistivity shows an increased tendency towards saturation at low temperature with substitution, while the NFL behavior observed in the unsubstituted sample at low temperature is only partially suppressed as far as electrical transport properties and specific heat are concerned. The power law divergence sets in at a much higher temperature compared to T_K, suggesting a two-fluid system with magnetically ordered rare regions coexisting with Kondo-screened metallic paramagnetic regions. While the macroscopic magnetic susceptibilities are more sensitive to Griffiths singularities arising out of interimpurity interaction, the resistivity and specific heat are dominated by local Fermi liquid components, except at very low temperatures.

III. SUMMARY

To conclude, we observed universal scaling of Kondo resistivity as well as magnetoresistance along with enhancement of Kondo and RKKY couplings with local moment Cr^{3+} substitution at the Ir sublattice. However, both the Kondo resistivity and specific heat show a deviation from Fermi liquid behavior at low temperature. The low-temperature magnetic susceptibility for $0 \leqslant x \leqslant 0.3$ is not described as a local Fermi liquid but is characterized by a power law divergent behavior, where $\chi \propto T^{-\xi_L}$, with the exponent $0.50 \leqslant \xi_L \leqslant 0.76$ being significantly less than unity. The magnetization at finite temperature T and nonzero magnetic field H exhibits a scaling of $(M/H)T^{\xi_L}$ as a universal function of H/T^{β}. The susceptibility at high temperature for the doped samples also follows power law divergence, with the exponent varying roughly in the range $0.8 \leqslant \xi_H \leqslant 0.9$. The observed non-Fermi liquid behavior is attributed to magnetically ordered rare regions, or the so-called Griffiths singularities, close to the quantum critical point.

ACKNOWLEDGMENT

We acknowledge the Department of Science and Technology (DST), government of India, for financial support.

[1] W. Witczak-Krempa, G. Chen, Y. Baek Kim, and L. Balents, Annu. Rev. Condens. Matter Phys. **5**, 57 (2014).
[2] D. Pesin and L. Balents, Nat. Phys. **6**, 376 (2010).
[3] J. S. Gardner, M. J. P. Gingras, and J. E. Greedan, Rev. Mod. Phys. **82**, 53 (2010).
[4] X. Wan, A. M. Turner, A. Vishwanath, and S. Y. Savrasov, Phys. Rev. B **83**, 205101 (2011).
[5] Y. Machida, S. Nakatsuji, S. Onoda, T. Tayama, and T. Sakakibara, Nature (London) **463**, 210 (2010).
[6] J. G. Rau, E. K-H. Lee, and H-Y. Kee, Annu. Rev. Condens. Matter Phys. **7**, 195 (2016).
[7] R. Schaffer, E. K.-H. Lee, B.-J. Yang, and Y. B. Kim, Rep. Prog. Phys. **79**, 094504 (2016).
[8] A. Juyal, A. Agarwal, and S. Mukhopadhyay, Phys. Rev. B **95**, 125436 (2017).
[9] A. Juyal, A. Agarwal, and S. Mukhopadhyay, Phys. Rev. Lett. **120**, 096801 (2018).
[10] R. Flint and T. Senthil, Phys. Rev. B **87**, 125147 (2013).
[11] S. B. Lee, A. Paramekanti, and Y. B. Kim, Phys. Rev. Lett. **111**, 196601 (2013).
[12] S. Nakatsuji, Y. Machida, Y. Maeno, T. Tayama, T. Sakakibara, J. van Duijn, L. Balicas, J. N. Millican, R. T. Macaluso, and J. Y. Chan, Phys. Rev. Lett. **96**, 087204 (2006).
[13] Y. Machida, S. Nakatsuji, Y. Maeno, T. Tayama, T. Sakakibara, and S. Onoda, Phys. Rev. Lett. **98**, 057203 (2007).
[14] T. Kondo, M. Nakayama, R. Chen, J. J. Ishikawa, E.-G. Moon, T. Yamamoto, Y. Ota, W. Malaeb, H. Kanai, Y. Nakashima, Y. Ishida, R. Yoshida, H. Yamamoto, M. Matsunami, S. Kimura, N. Inami, K. Ono, H. Kumigashira, S. Nakatsuji, L. Balents, and S. Shin, Nat. Commun. **6**, 10042 (2015).
[15] T. Ohtsuki, Z. Tian, A. Endo, M. Halim, S. Katsumoto, Y. Kohama, K. Kindo, M. Lippmaa, and S. Nakatsuji, Proc. Natl. Acad. Sci. USA **116**, 8803 (2019).
[16] B. Cheng, T. Ohtsuki, D. Chaudhuri, S. Nakatsuji, M. Lippmaa, and N. P. Armitage, Nat. Commun. **8**, 2097 (2017).
[17] P. Telang, K. Mishra, G. Prando, A. K. Sood, and S. Singh, Phys. Rev. B **99**, 201112(R) (2019).
[18] Z. Porter, E. Zoghlin, S. Britner, S. Husremovic, J. P. C. Ruff, Y. Choi, D. Haskel, G. Laurita, and S. D. Wilson, Phys. Rev. B **100**, 054409 (2019).
[19] A. Ikeda and H. Kawamura, J. Phys. Soc. Jpn. **77**, 073707 (2008).
[20] S. Doniach, Phys. B+C (Amsterdam) **91**, 231 (1977).
[21] V. K. Dwivedi and S. Mukhopadhyay, J. Appl. Phys. **125**, 223901 (2019).
[22] V. K. Dwivedi and S. Mukhopadhyay, J. Appl. Phys. **126**, 165112 (2019).
[23] K. Matsuhira, M. Wakeshima, Y. Hinatsu, and S. Takagi, J. Phys. Soc. Jpn. **80**, 094701 (2011).
[24] V. K. Dwivedi, A. Juyal, and S. Mukhopadhyay, Mater. Res. Express **3**, 115020 (2016).
[25] J. N. Millican, R. T. Macaluso, S. N. Y. Machida, Y. Maeno, and J. Y. Chan, Mater. Res. Bull. **42**, 928 (2007).
[26] H. Takatsu, K. Watanabe, K. Goto, and H. Kadowaki, Phys. Rev. B **90**, 235110 (2014).

[27] M. B. Gamza, R. Gumeniuk, U. Burkhardt, W. Schnelle, H. Rosner, A. Leithe-Jasper, and A. Slebarski, Phys. Rev. B **95**, 165142 (2017).
[28] S. Lutkehoff, M. Neumann, and A. Slebarski, Phys. Rev. B **52**, 13808 (1995).
[29] H. Ishii, K. Obu, M. Shinoda, C. Lee, Y. Takayama, T. Miyahara, T. D. Matsuda, H. Sugawara, and H. Sato, J. Phys. Soc. Jpn. **71**, 156 (2002).
[30] A. Slebarski, M. Neumann, and S. Mahl, Phys. Rev. B **51**, 11113 (1995).
[31] N. Paunovic, Z. Dohcevic-Mitrovic, R. Scurtu, S. Askrabic, M. Prekajski, B. Matovic, and Z. V. Popovic, Nanoscale **4**, 5469 (2012).
[32] D. R. Hamann, Phy. Rev. **158**, 570 (1967).
[33] K. Fischer, Z. Phys. **225**, 444 (1969).
[34] Y. P. Singh, D. J. Haney, X. Y. Huang, I. K. Lum, B. D. White, M. Dzero, M. B. Maple, and C. C. Almasan, Phys. Rev. B **89**, 115106 (2014).
[35] M. D. Daybell and W. A. Steyert, Phys. Rev. Lett. **20**, 195 (1968).
[36] J. S. Schilling and W. B. Holzapfel, Phys. Rev. B **8**, 1216 (1973).
[37] P. W. Anderson and G. Yuval, Phys. Rev. Lett. **23**, 89 (1969).
[38] T. Moriya and T. Takimoto, J. Phys. Soc. Jpn. **64**, 960 (1995).
[39] S. Watanabe and K. Miyake, Phys. Rev. Lett. **105**, 186403 (2010).
[40] A. Schröder, G. Aeppli, R. Coldea, M. Adams, O. Stockert, H. v. Löhneysen, E. Bucher, R. Ramazashvili, and P. Coleman, Nature (London) **407**, 351 (2000).
[41] G. R. Stewart, Rev. Mod. Phys. **73**, 797 (2001).
[42] D. T. Adroja, A. D. Hillier, J.-G. Park, W. Kockelmann, K. A. McEwen, B. D. Rainford, K-H. Jang, C. Geibel, and T. Takabatake, Phys. Rev. B **78**, 014412 (2008).
[43] B. Andraka and G. R. Stewart, Phys. Rev. B **47**, 3208 (1993).
[44] I. Affleck and A. W. W. Ludwig, Phys. Rev. B **48**, 7297 (1993).
[45] A. H. Castro Neto, G. Castilla, and B. A. Jones, Phys. Rev. Lett. **81**, 3531 (1998).
[46] B. Andraka and A. M. Tsvelik, Phys. Rev. Lett. **67**, 2886 (1991).